2.9 Interaction Region for the FCC-ee Design

M. Boscolo
INFN-LNF, Via E. Fermi, 40 I-00044 Frascati (Rome), Italy;
M.K. Sullivan
SLAC, Menlo Park, California 94025, USA
Mail to: manuela.boscolo@lnf.infn.it, sullivan@slac.stanford.edu

2.9.1 Introduction

We present here a current snapshot of the Interaction Region (IR) design for the Future Circular Collider electron-positron accelerator (FCC-ee) [1]. We introduce the IR design based on accelerator requirements and describe the additional details important in the study of backgrounds in the detector as well as to the needs of the detector. The requirements of the detector and of the accelerator at the collision point together make the IR one of the more challenging parts of the overall design. The challenge is to maximize performance in terms of integrated luminosity and minimize beam related backgrounds for the experiments. This includes minimizing synchrotron radiation in the IR.

2.9.2 Present IR design

2.9.2.1 *Accelerator Parameters used in the IR*

We list in Table 1 below the most important accelerator parameters used in designing the IR. We note in particular the high beam current and high luminosity of the Z operating point. The B-factories (PEP-II and KEKB) had such high beam currents but only about 1% of the luminosity. Even so, the B-factories had significant backgrounds from luminosity processes, in particular, radiative Bhabhas. On the other hand, the $t\bar{t}$ operating point while having low beam currents has the highest beam energy of 182.5 GeV and therefore the highest photon energy spectra from Synchrotron Radiation (SR).

The crab-waist collision scheme [2,3] associated with a large Piwinski angle and a very low vertical beta function has been chosen for the FCC-ee design. This scheme reduces the hourglass effect, allowing the vertical beta function β_y at the interaction point (IP) to be smaller than the bunch length. There is a net luminosity gain due to the small beam size at the interaction point and this gain is obtained with lower beam currents than those required for a conventional collision scheme. This scheme requires a large Piwinski angle, obtained with a small horizontal beam size and a large crossing angle (30 mrad). The large crossing angle at the interaction point allows for the beams to enter/exit separate beam pipes at about ±1.2 m after the IP. So, the initial final focus defocusing quadrupole (QC1) can be a separate magnet for each beam. There is about 6 cm of space between the beams at the face of QC1 (±2.2 m).

One of the most significant consequences of this large crossing angle scheme at the IP is the large bending of the incoming and outgoing beam trajectories in order to achieve this large angle. To minimize the effect on the IR of SR fans from these bend magnets we use an asymmetric optics such that the inner ring goes into the IP with soft upstream bend magnets. The beam is then bent more strongly after the IP in order to merge back close to the incoming beam ring.

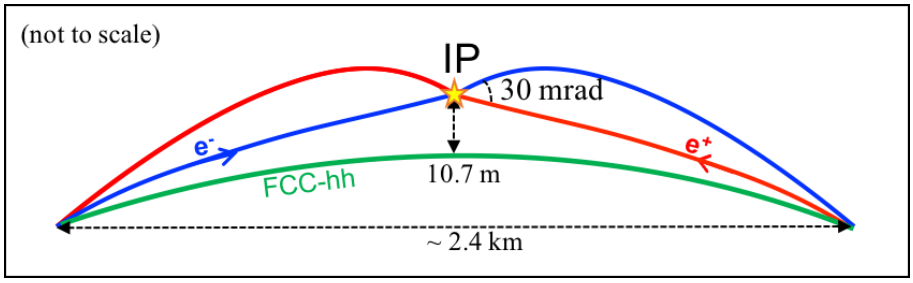

Figure 1: Sketch of the FCC-ee beam trajectories at IR.

Figure 1 shows a not-to-scale sketch of the FCC-ee IR together with the FCC hadron (FCC-hh) collider trajectory. The tunnel is defined by the FCC-hh design, and FCC-ee design has to adapt its layout to this footprint. The green line in the plot is the FCC-hh trajectory and in red and blue are the $e^+$and e^- trajectories, asymmetric with respect to the IP. The distance between the FCC-ee IP with FCC-hh beamline is 10.7 m. Outside the IR, the FCC-ee and FCC-hh trajectories are on the same orbit. However, inside the FCC-ee IR, an additional tunnel is necessary for ±1.2 km around the IP in order to allow for the crab-waist collision scheme with a large crossing angle. The interaction region is nevertheless locally symmetric, as is shown in Figure 3 and will be discussed in the next section.

Table 1: FCC-ee accelerator parameters that influence the IR design [4].

	Unit	***Z***	***WW***	***Higgs***	***tt̄***
Circumference	km	97.756			
Crossing angle	mrad	30			
L*	m	2.2			
Beam Energy	GeV	45.6	80	120	182.5
Beam current	mA	1390	147	29	5.4
Number of Bunches	#	16640	2000	393	39
Particles/bunch	$\times 10^{10}$	17	15	15	28
Hor. emittance	nm-rad	0.27	0.28	0.63	1.45
Ver. emittance	pm-rad	1.0	1.0	1.26	2.68
β_x at IP	m	0.15	0.2	0.3	1.0
β_y at IP	mm	0.8	1.0	1.0	2.0
σ_x at IP	μm	6.4	7.5	13.8	38.1
σ_y at IP	nm	28	32	36	73
Bunch length (SR/BS)	mm	3.5 / 12.1	3.3 / 7.65	3.15/4.9	2.5/3.3
Energy spread (SR/BS)	%	0.038 / 0.132	0.066 / 0.153	0.099 /0.151	0.15 / 0.20
Energy acceptance	%	1.3	1.3	1.5	2.5
Luminosity	$\times 10^{34}$	230	32	7.8	1.5

Crab sextupoles are the other ingredient of this scheme. They rotate the β_y function so that its waist is on the central trajectory of the opposite colliding beam and, in addition, they suppress betatron and synchro-betatron resonances introduced by the large Piwinski

angle. These crab sextupoles have to be at the proper phase advance with respect to the IP (0.5 π and π for the vertical and horizontal plane, respectively) and with the proper strength $k = \frac{1}{\theta}\frac{1}{\beta_y^* \beta_y}\sqrt{\frac{\beta_x^*}{\beta_x}}$. The FCC-ee IR implements this collision scheme at very high energy, so the design has to cope with high synchrotron radiation induced by incoming bending trajectories at the IR. The optics that minimizes SR fans into the experiments is asymmetric for the bending magnets as well as for the sextupoles needed for the vertical chromaticity correction.

The design of the beam optics is described in Refs. [5,6] and we refer here to lattice version 208_nosol [7]. The current IR design (below) attempts to accommodate all operating points for the accelerator, so the IR optics is rescaled in energy and the β functions at IP are optimized for each running energy. In fact, to mitigate the coherent beam-beam instabilities at the Z [8] the β_x^* is reduced to 15 cm with respect to 1 m at the $t\bar{t}$ energy. β_y^* goes from 0.8 mm at the Z to 2 mm at the $t\bar{t}$. On the other hand, at highest energies the beamstrahlung effect is stronger, limiting the beam lifetime. Thus, at the highest energy run, the required energy acceptance is larger (2.5%) due to the increase of the energy spread. Top-up injection is also planned in order to increase efficiency and manage with a beamstrahlung lifetime of less than one hour.

Figure 2 shows the $\sqrt{\beta_x}$, $\sqrt{\beta_y}$ and dispersion functions before 900 m and after 500 m from the IP for the top energy ($t\bar{t}$). It can be seen that the IR optics is asymmetric. The last bending magnet before the IP ends at about 114 m from the IP while the first bending magnet after the IP is as close as 25 m.

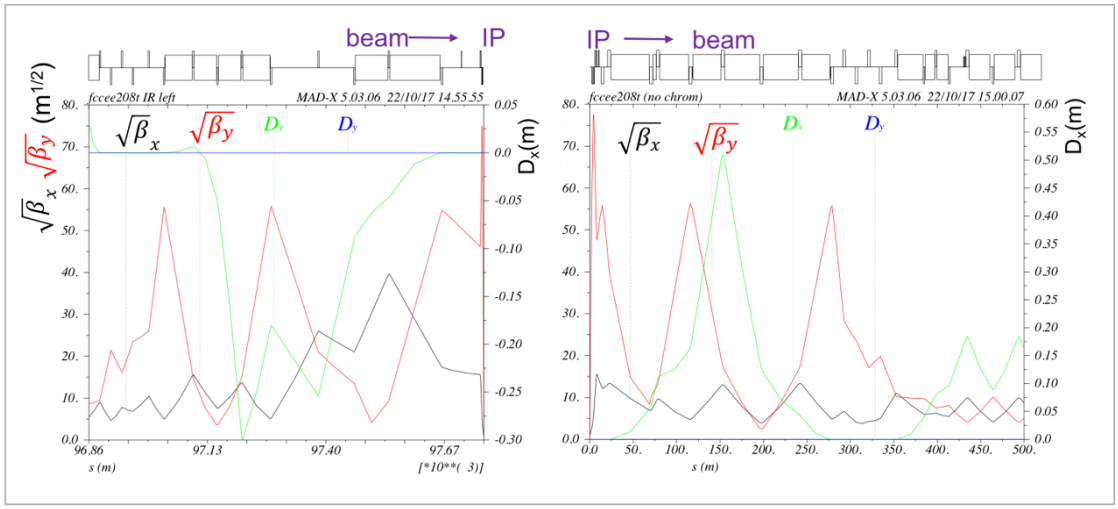

Figure 2: $\sqrt{\beta_x}$ and $\sqrt{\beta_y}$ functions and dispersion from 900 m to the IP (left) and from the IP to 500 m (right).

2.9.2.2 *The Interaction Region Layout*

Figure 3 displays the current interaction region layout in an expanded horizontal scale in order to show more detail in the X dimension. The face of the final focus magnets is 2.2 m from the Interaction Point (IP) which is the definition of L* in Table 1. The final focus magnets are super-conducting and there is a compensating solenoid for the detector magnetic field located from 1.25 to 2.2 m from the IP on either side. Just in front of the

compensating solenoids is a luminosity calorimeter designed to precisely measure the collision luminosity (LumiCal) especially at the Z operating point. It is shown in magenta in the plot. The absolute precision of luminosity at the Z energy is required to be 10^{-4}, requiring an alignment on the order of μm. The support of this monitor is not designed yet. Full background simulation with a Geant4 model of the IR is under study [9] and preliminary results indicate that the beam background impact on the luminosity monitor is under control and the luminosity precision can be reached.

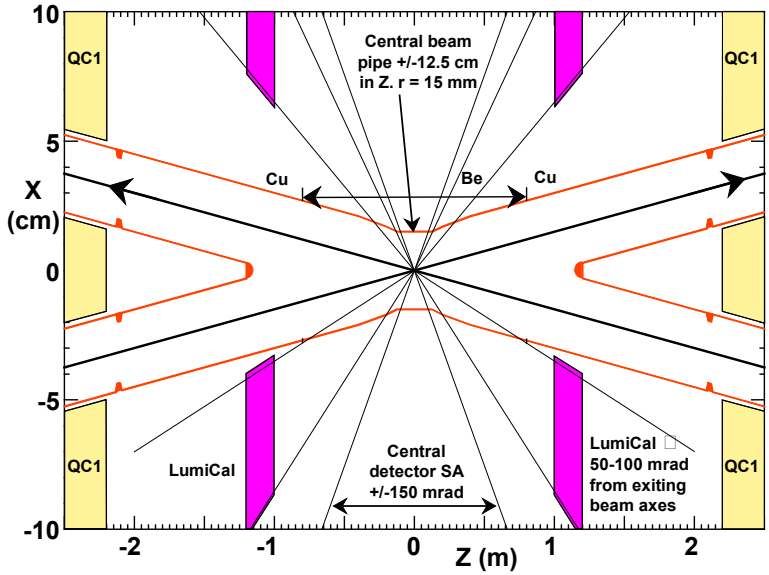

Figure 3: Layout of the IR design. Note the expanded horizontal scale. The central chamber is made of Be with a thin coating of Au (~5 μm) on the inside to absorb scattered low-energy photons from the synchrotron radiation fans of the last bend magnet. The detector axis is parallel to the Z axis and the detector magnetic field is also parallel to the Z axis.

The super-conducting final focus magnets will also have screening solenoids on the outside of the magnets in order to cancel the 2 T detector magnetic field and the compensating solenoid in front of the final focus magnets is approximately twice the detector field strength with opposite sign in order to cancel the total remaining integral of the detector field between the final focus magnets. The detector magnetic field is set to 2 T in order to keep the vertical emittance blow-up at an acceptable value. This solenoid compensation scheme limits the increase of the vertical emittance to about 30% of its nominal value, which is of the order of a pm [10].

Two separate beam pipes host the two beams and only in the IR are they merged together into a single vacuum chamber. Two experiments are foreseen, at opposite sides. The beam pipe is circular with circular masks. It has a diameter of 3 cm from ±5.6 m around the IP except where the beam pipes merge into one central beam pipe. From ±5.6 to ±8.2 the beam pipe has a 4 cm diameter. Beyond ±8.2 m from the IP the beam pipe has a 6 cm diameter. These values can be compared to the horizontal and vertical beam sizes shown in Figure 4. The maximum vertical beam size happens in the middle of the first defocusing quadrupole QC1, here 60 σ_y correspond to 7.6 mm (well within 30 mm). In the final focus region the horizontal beam size is largest at the back end of the final focus focusing quadrupole QC2 , where σ_x = 0.6 mm and 20 σ_x correspond to 12 mm, to be compared to the radius of the circular aperture. The horizontal beam size increases in the

last dipole at about 150 m before the IP, in this location 20 σ_x correspond to 30 mm, but the pipe is 60 mm.

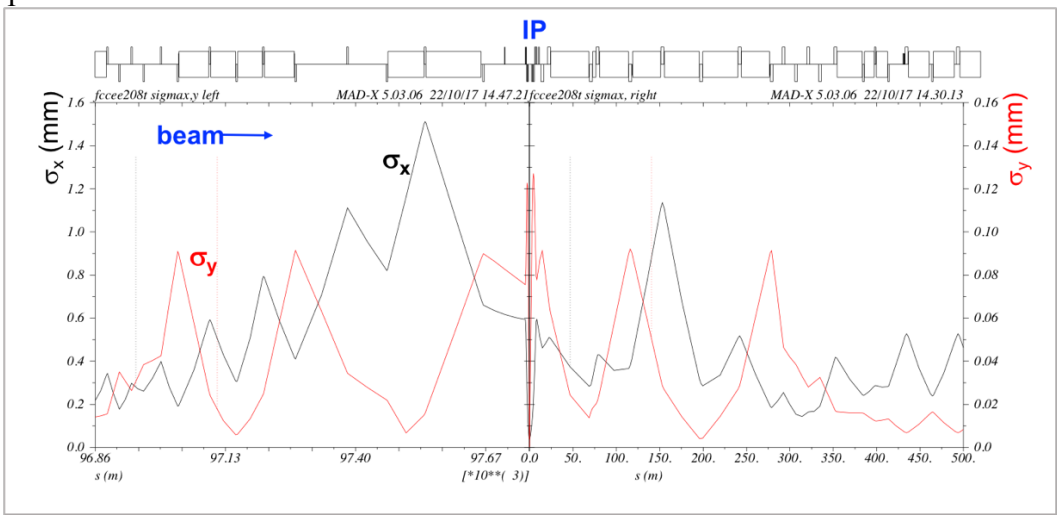

Figure 4: Beam sizes upstream –900 m and downstream +500 m from the IP for the top energy for a $\Delta p/p$=0.2%. Left and right axis refer to σ_x and σ_y in mm.

The complicated geometry of the region where the two beam pipes are merged together keeping a constant aperture of 3 cm has been designed with CAD and checked with CTS and HFSS codes to analyse electro-magnetic fields in the IR (see Figure 5). These studies show that the cut-off frequency of electro-magnetic fields generated or trapped in the IR is at a safe value. High order mode absorbers have also been designed following the PEP-II experience [11]. The beam pipe will be at room temperature and water cooling is foreseen to mainly cool the area where HOM are placed due to the absorption of deposited power and where the SR masks are located.

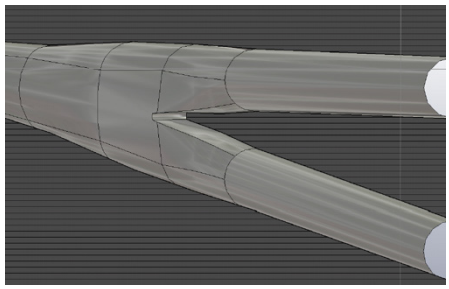

Figure 5: Smooth geometrical transitions from double to single vacuum pipe [13].

The beam pipe will be made of copper with an optimized coating to control the electron cloud build up and the transverse and longitudinal impedances [12]. However, the beam pipe of the central region (±0.9 m from the IP), which includes the luminosity monitor window, needs to be made from a low-Z material like Beryllium (Be) (see Fig. 3). In addition, the central Be chamber will need to be cooled especially during the high-current Z running.

2.9.3 SR backgrounds from the last bend magnet before the IR

The possible sources of background from SR come from the last bending magnet before the collision point and from the quadrupoles between the bending magnet and the

IP. In order to minimize SR backgrounds from the last bend magnet we have requested the magnetic field to be as low as possible and near 100 keV for the critical energy of the bend radiation coming from this bend field out to 500 m from the IP. This requirement comes after the LEP2 experience, where the highest experimental limit was a critical energy of 72 keV from 260 m to the IP [13], which resulted in manageable detector backgrounds. The last bend magnet before the IP will always send a beam of SR photons down into the IR. In order to minimize this radiation fan the last bend magnet is approximately positioned between 100 and 200 m upstream of the collision point. Nevertheless, at the $t\bar{t}$ beam energy this radiation fan is the dominant source of SR background for the detector. We have placed SR mask tips at 2.1 m upstream of the IP, just in front of the first final focus defocusing quadrupole, in order to intercept this radiation fan and prevent the photons from directly striking the central Be beam pipe. The next level of SR background then comes from photons that strike near the tip of these masks, forward scatter through the mask and then strike the central beam pipe. At the $t\bar{t}$ energy, most of these scattered photons will penetrate the Be beam pipe and then cause backgrounds in the detector. To reduce the effect of this SR source on the experiment we propose to add a thin layer of high-Z material, for example gold, to the inside of the Be beam pipe. This is under study and we have found that at the top energy any reasonable thickness of gold (up to 10 μm) is not very effective due to the high energy of the scattered photons from the mask tip while at the Z energy the tip-scattered photons are so few and so soft that a gold layer is probably not needed. However, a layer of high conductivity metal will be needed (especially at the Z) in order to minimize beam pipe heating from image charge currents. Table 2 is a partial summary of the SR study up to now with details about the photon rate from the mask tip and the hit rate on the inside of the central Be beam pipe for the four different beam energies of the FCC-ee. This Table gives only the number of SR photons incident on the very central part of the IR Be beam pipe (±12.5 cm). Full GEANT4 studies (which include a model of the entire beam pipe and of the nearby sub-detectors) of the scattered photons from these mask tips are needed and are underway with very encouraging preliminary results [9]

Synchrotron radiation adds an additional requirement on the overall optics design by requiring the critical energy throughout the ring to be no higher than 1 MeV in order to minimize the effects of neutron production via the giant dipole resonance. A complete description of the approach used to study and control the SR in the FCC-ee IR is in Ref. [15].

Table 2: Synchrotron Radiation background calculations for the fan from the last upstream bend magnet. The central beam pipe is a cylinder ±12.5 cm in Z with a radius of 15 mm.

Number of photons	***Z***	***WW***	***Higgs***	$t\bar{t}$
Per bunch from the last bend magnet	6.69×10^{10}	1.03×10^{11}	1.55×10^{11}	1.37×10^{13}
Total incident on mask at 2.1 m	4.93×10^{8}	7.61×10^{8}	1.15×10^{9}	3.27×10^{9}
Incident on mask > 1 keV	7.38×10^{7}	3.33×10^{8}	7.00×10^{8}	2.41×10^{9}
Scattered from the mask tip > 1 keV	8	9390	2.58×10^{5}	$7.87\text{x}10^{6}$
Inc. on the central beam pipe > 1 keV	< 0.0037	< 0.033	3	787
Critical energy of bend radiation (keV)	1.63	8.45	28.5	100

2.9.4 SR backgrounds from the final focus quadrupoles

The final focus quadrupoles are very powerful in order to focus the beam to the required small spot at the collision point. This means the beta functions inside these quadrupoles are very large and therefore some fraction of beam particles experience very high magnetic fields in these magnets. The result of this is that the 4 quadrupoles (2 upstream and 2 downstream of the IP) for each beam generate quite intense (2.09 kW at $t\bar{t}$), very high energy photon beams that exit the IR. These photon beams will eventually strike the vacuum chamber as it bends with the outgoing beam as the beam goes through the downstream bending magnet. Although the photons in these SR beams have a rapidly falling energy spectrum there are still a significant number of photons greater than 1 MeV at the $t\bar{t}$ beam energy and some fraction of these photons could excite the giant dipole resonance. This will require a detailed study in order to understand and perhaps protect the detector from a possible nearby source of neutron background.

2.9.5 Other beam related backgrounds

The IR has been modelled starting from the CLIC detector design using Geant4 for full simulation of all the subdetectors. The effects of IP backgrounds such as radiative Bhabha, beamstrahlung, e^+e^- pair production and $\gamma\gamma$ to hadrons are being studied in terms of hit density, occupancy and deposited energy.

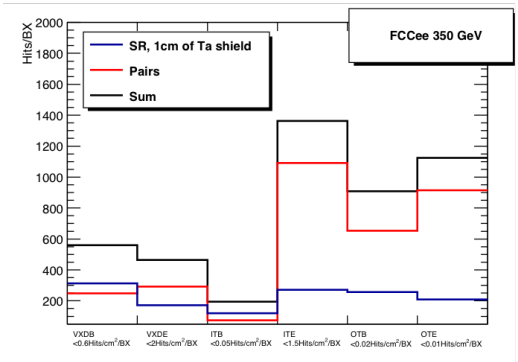

Figure 6: Hits per subdetector per bunch crossing. The plot shows the importance of a high-z shielding (in this case Tantalum [Ta]) around the beam pipe where possible (blue line).

An additional relevant source of beam related backgrounds in the detector can be beam-gas scattered particles (beam-gas bremsstrahlung and Coulomb scattering). Simulation studies are in progress, and preliminary results indicate that these sources are under control. Touschek scattering can in principle induce detector background from the small intense beam size in the IR. However, due to the high beam energy, this effect is not dominant as it is for low energy colliders. We see from Table 2 that SR backgrounds are clearly most important for the $t\bar{t}$ energy machine and that these backgrounds rapidly diminish as the beam energies go down. We actually see essentially no background from SR at either the Z or the WW machines. However, as the beam current increases with decreasing beam energy the lost beam particle backgrounds will become more significant and a careful study of the vacuum pressure along with collimator placement around the

rings will become very important. In addition, with the decrease in beam energy there is also an increase in luminosity and for the lower energy machines the luminosity backgrounds (radiative Bhabha, e+e- pair production, $\gamma\gamma$ to hadrons…) will dominate. At the $t\bar{t}$ energy one major concern is beamstrahlung which also determines the beam lifetime.

2.9.6 **Conclusion**

We have described the IR layout of the FCC-ee collider, a challenging and innovative machine that aims at precision studies and rare decay observations in the range of 90 to 365 GeV centre-of-mass energy. We have shown the key challenges but also the feasibility of the design.

We have discussed the constraints of the design imposed by the beam optics, the parameter choices and the collision scheme, together with the physics requirements, the luminosity measurement precision, and backgrounds, in particular synchrotron radiation. Synchrotron radiation is in fact a major contributor to this layout and we have shown the countermeasures that reduce this effect to manageable levels.

2.9.7 **Acknowledgements**

The authors wish to thank M. Benedikt, H. Burkhardt, A. Kolano, R. Kersevan, M. Koratzinos, K. Oide, G. Voutsinas, F. Zimmermann for useful discussions and suggestions.

2.9.8 **References**

1. The FCC-ee study, http://cern.ch/fcc .
2. P. Raimondi, D. Shatilov, M. Zobov, arXiv:physics/0702033 (2007).
3. M. Zobov *et al*., PRL **104**, 174801 (2010).
4. A. Blondel, P. Janot, K. Oide, D. Shatilov, F. Zimmermann, FCC-ee parameter update, 6 October (2017).
5. K. Oide *et al.*, Phys. Rev. Accel. Beams **19** (2016) no.11, 111005.
6. K. Oide *et al.*, in Proc. IPAC17, TUOCB1, Copenhagen, May 2017.
7. K. Oide, private communication, October 2017.
8. K. Ohmi, N. Kuroo, K. Oide, D. Zhou and F. Zimmermann, Phys. Rev. Lett. **119** (2017) no.13, 134801.
9. G. Voutsinas, N. Bacchetta, P. Janot, A. Kolano, E. F. Perez, N.A. Tehrani, M. Boscolo, M.K. Sullivan, in Proc. IPAC17, WEPIKP004, Copenhagen, May 2017. See also presentation at the FCC WEEK 2017.
10. S. Sinyatkin, M. Koratzinos, presented at the FCC-ee MDI workshop, January (2017), https://indico.cern.ch/event/596695
11. A. Novokhatski, this ICFA edition.
12. E.~Belli *et al.,* in Proc. IPAC17, THPAB020, Copenhagen, May 2017.
13. Courtesy of Miguel Gil Costa, May (2017).
14. G. von Holtey *et al.*, Nucl. Instrum. Meth. A 403 (1998) 205.
15. M. Boscolo, H. Burkhardt and M. Sullivan, Phys. Rev. Accel. Beams **20** (2017) no.1, 011008.